Observation of Nonlinear Propagation of Spin-Entropy Wave in Superfluid ^{3}He

M. Bastea, H. Kojima, and P. G. N. deVegvar*
Serin Physics Laboratory, Rutgers University, Piscataway, New Jersey 08854
(Received 5 January 1996)

The propagation of a spin-entropy wave in superfluid ^{3}He-A_1 was observed in a cylindrical chamber with the magnetic field applied perpendicular to the chamber axis. A strong nonlinear response was observed as a function of drive amplitude. When the drive is relatively small, the resonant response is hysteretic and is dependent on the direction of frequency sweep through the resonance. When the drive is increased to a sufficiently large value, the response reverts to nearly linear dependence.

PACS numbers: 67.57.De, 47.37.+q, 67.57.Fg

A chamber containing anisotropic superfluid phases of ^{3}He provides an intricate laboratory system in which simultaneously broken symmetries in gauge, orbital, and spin space can be studied [1]. One consequence of the broken symmetries is that the measured superfluid component density depends on the direction and magnitude of the imposed superflow, the cell geometry, and applied magnetic field. There have been numerous theoretical and experimental studies on the "textures" of the orbital symmetry vector in ^{3}He-A phase in which NMR is an excellent probe. There have been few experimental studies related to orbital anisotropy in the spin-polarized superfluid ^{3}He-A_1 phase except for an early ultrasonic attenuation measurement [2]. The spin-entropy (second sound) wave propagation is a probe sensitive to textures in the A_1 phase. In this Letter we report on the first observations of nonlinear propagation of the spin-entropy wave. We show that the nonlinearity originates from the effects of superflow amplitude on the texture, which in turn changes the propagation velocity. Unexpectedly, the nonlinearity does not continue to grow but the propagation reverts to a quasilinear behavior at high drive amplitudes. The nonlinearity is so severe that it occurs at velocities well below the onset of critical velocity effects. Comparisons to mechanical model systems and texture patterns obtained from free energy considerations are found to be consistent with these observations.

The usefulness of spin-entropy wave in studying textural effects may be seen from the expression for its velocity [3] given to a good approximation by

$$\mathbf{C}(\hat{\mathbf{q}})_{se}^2 = \left[\frac{\rho_s}{\rho_n}\right]_{\alpha\beta}\left(\frac{\rho}{\chi}\right)\left(\frac{\hbar\gamma}{2m}\right)^2 \hat{\mathbf{q}}_\alpha \hat{\mathbf{q}}_\beta , \qquad (1)$$

where $\hat{\mathbf{q}}$ is the unit wave vector, ρ the total mass density, χ magnetic susceptibility, γ gyromagnetic ratio, and m the mass of ^{3}He. The propagation velocity depends on the texture through the superfluid to normal component density ratio $(\boldsymbol{\rho_s}/\boldsymbol{\rho_n})$, which is a direction $(\hat{\mathbf{q}})$ dependent quantity. Given a texture $\hat{\mathbf{l}}$, the superfluid density may be expressed as

$$[\rho_s]_{\alpha\beta} = \rho_{s\parallel}(2\delta_{\alpha\beta} - \hat{\mathbf{l}}_\alpha \hat{\mathbf{l}}_\beta)\hat{\mathbf{q}}_\alpha \hat{\mathbf{q}}_\beta , \qquad (2)$$

where $\rho_{s\parallel}$ is the superfluid density measured along $\hat{\mathbf{l}}$ [4]. The textural pattern of θ $[\theta = \cos^{-1}(\hat{\mathbf{l}} \cdot \hat{\mathbf{q}})]$ is in general determined by minimizing the total free energy contributions from the dipolar, bending, and flow energy subject to the constraint that $\hat{\mathbf{l}}$ be perpendicular to the walls. The spin-entropy wave velocity is thus intimately related to the $\hat{\mathbf{l}}$ vector texture.

The resonant spin-entropy wave propagation apparatus is similar to the one described earlier [5] except for one crucial difference. The cell containing the resonator was entirely reconstructed such that the resonator axis was rotated by 90°. Thus the external magnetic field $\mathbf{H}$ is now perpendicular to the spin-entropy wave vector $\hat{\mathbf{q}}$. This change in orientation made it possible to observe the nonlinear effects presented below. As before, oscillating superleak membrane capacitive transducers [6] are used to drive and detect the spin-entropy wave resonances in a cylindrical chamber (radius = 4 mm, length = 12.7 mm, $\hat{\mathbf{q}} \parallel$ axis). The detector is dc voltage biased with $V_{\rm dc}$ and the motion of the membrane induces a voltage which is measured by a lock-in amplifier. A separate dc bias plus ac voltage, $D\cos\omega t$, is applied to the drive. ^{3}He could easily be cooled into the A_1 phase and the warm-up rate was about 1 nK/s. The liquid pressure was fixed at 22.9 bars where $T_c = 2.315$ mK and $(T_{c1} - T_{c2})/B = 50.9\ \mu$K/T [7]. A melting curve thermometer and a vibrating wire served as temperature sensors.

Examples of the measured response of the fundamental mode [8] are shown in Figs. 1(a)–1(c) for $D = 1.15$ V and in Figs. 1(d)–1(f) for $D = 2.6$ V in a magnetic field of 4 T. The temperature is about 13% of $T_{c1} - T_{c2}$ above T_{c2} and is just outside of the anomalous attenuation region [5]. The measured quadrature signals, x and y, and computed magnitude M $(= \sqrt{x^2 + y^2})$ are shown for the two directions of frequency sweep. Note the clear hysteretic response depending on the direction of sweep in Figs. 1(a)–1(c). The response is reproducibly observed, is not due to temperature change between the two sweeps, and does not depend on the order of the sweep direction. For each direction of sweep, the signal changes abruptly and passes through maximum magnitudes, $M_{\rm up}$ and $M_{\rm down}$, at clearly identifiable frequencies, $f_{\rm up}$ and $f_{\rm down}$. For

 0031-9007/96/76(15)/2766(4)$10.00

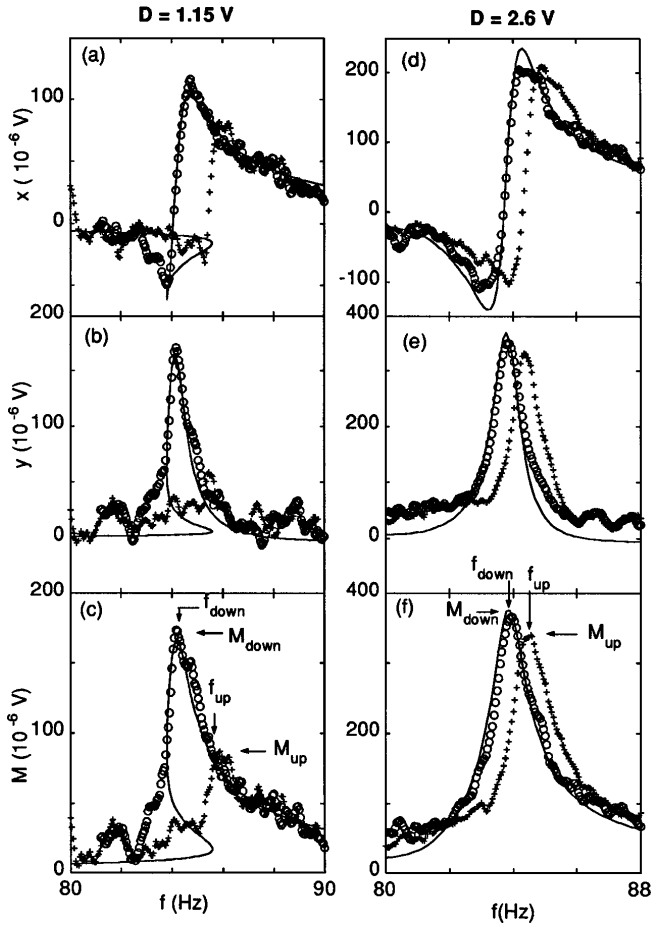

FIG. 1. Measured hysteretic "in" (x) and "out" (y) of phase and magnitude (M) signals at drive amplitude $D = 1.15$ V, (a)–(c), and 2.6 V, (d)–(f), for increasing (crosses) and decreasing (circles) frequency sweeps. The lines represent response of a nonlinear mechanical oscillator. See text.

D less than 1.15 V, the response becomes even more abrupt at f_{up} and f_{down}. As D is increased beyond about 1.6 V, the abruptness gradually diminishes. Though they no longer locate the abrupt changes, the f's and M's are defined as indicated in Fig. 1(f). In the high drive limit [Figs. 1(d)–1(f)], though there is a slight shift between the two sweep directions, the response is nearly that of a linear system. This change, from nonlinear to linear response as the drive level is increased, is surprising.

Qualitatively similar responses to those in Fig. 1 (and in Fig. 2 below) are observed in the temperature range $0.87 < (T_{c1} - T)/(T_{c1} - T_{c2}) < 0.30$. The range extends to well outside the region of the anomalous spin-entropy wave attenuation above T_{c2} previously reported [5]. Thus we believe that the nonlinear effects reported here are not closely related to the anomalous attenuation. Apparently the nonlinear effects do not depend strongly on the superfluid fraction (which varies by a factor of 2 in the observed temperature range).

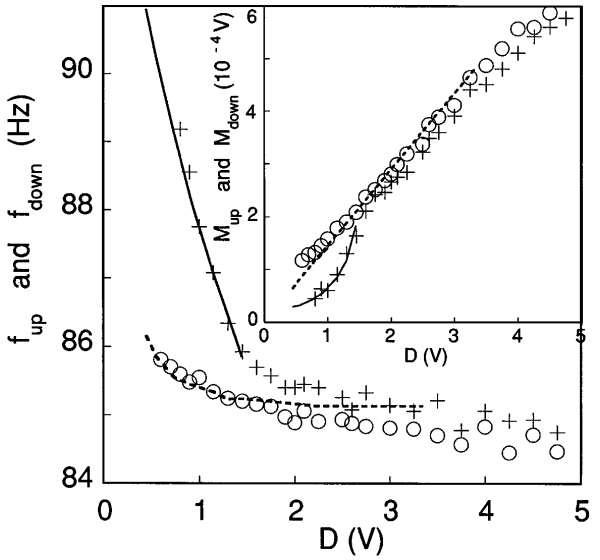

FIG. 2. Measured frequencies [f_{up} (crosses) and f_{down} (circles) as defined in Fig. 1] where abrupt changes in response take place as a function of drive amplitude. The inset shows the measured magnitudes, M_{up} (crosses) and M_{down} (circles) as function of drive amplitude in the same measurement. The solid and dotted lines represent the corresponding quantities for a nonlinear mechanical oscillator. See text.

The sensitivity of the capacitive oscillating superleak transducers used here was analyzed theoretically [6]. Under the simplifying assumption that the "liquid stiffness" is much greater than that of the membrane, the superfluid component velocity in the first mode is related to the measured amplified voltage M by $v_s \cong (Q/4\pi)(M/\Gamma V_{\mathrm{dc}})\rho C_{se}/\rho_s$. Here Q is the quality factor and Γ is the amplifier gain. Inserting the appropriate values for the data in Figs. 1 and 2 ($Q = 90$, $\Gamma = 100$, $V_{\mathrm{dc}} = 160$ V, $\rho_s/\rho = 8 \times 10^{-3}$, $C_{se} = 2.1$ m/s) gives $v_s/M = 0.12$ (m/s)/V.

The measured drive dependences of f_{up}, f_{down}, M_{up}, and M_{down} are shown in Fig. 2. The figure illustrates the highly nonlinear behavior at low drive levels and essentially linear behavior at high drive levels. While there is little drive dependence to f_{down}, the drive dependence of f_{up} is much greater. Evidence of nonlinearity is perhaps most dramatic in the drive dependence of M_{up}. As D is decreased below 1.6 V, M_{up} decreases sharply deviating from the linear response at greater D. On the other hand, M_{down} is almost proportional to D over all of the measured range. When D is decreased below 0.5 V, the resonant response becomes unstable and irreproducible from one set of sweeps to another. This, and not the noise level, is responsible for the lack of M_{down} data in this range. The texture seems to fluctuate and a stable one does not seem to be established by the small superflows. The low superflow limit will be further investigated in future studies. It should be emphasized that these

hysteretic and nonlinear responses were not observed when $\mathbf{H} \parallel \hat{\mathbf{q}}$ [5].

The qualitative features of the observed nonlinear behavior of spin-entropy wave may be explained as follows. Given the magnetic field applied to ^{3}He contained within the resonator and a small superflow (due to a residual heat leak), the fluid should stabilize to an "undisturbed" $\hat{\mathbf{l}}$ and $\hat{\mathbf{d}}$ texture pattern. Generating spin-entropy waves imposes oscillatory probe superflows in the chamber. If the probe superflow is so weak that the texture is not modified, the measured speed of the spin-entropy wave is determined by the undisturbed texture. In the present experiment, this weak flow limit is not observed. As the probe superflow is increased, the superflow begins to align $\hat{\mathbf{l}}$ in the region away from the walls towards the flow direction, thereby decreasing the kinetic energy contribution to the free energy (see below). This change in texture decreases the effective superfluid fraction "seen" by the spin-entropy wave and therefore its speed. The flow-induced texture transformation leads to the observed "soft" nonlinear response. As the superflow velocity is increased further, the region of $\hat{\mathbf{l}}$ alignment spreads towards the walls. Since $\hat{\mathbf{l}}$ is constrained to be perpendicular to the walls, this requires sharper bending hence greater bending energy. As the cost in bending energy becomes greater, the flow-induced alignment tends to saturate. In this large flow limit the response reverts to linearlike behavior as observed in the experiment.

The mechanism of the nonlinearity just described may be modeled by a driven spring-mass oscillator whose spring constant decreases as the amplitude is increased [9]. An equation of motion given by $\ddot{z} + k\dot{z} + az(1 + bz^2)/(1 + cz^2) = G\cos\omega t$ describes such a nonlinear oscillator [10]. Here z is the displacement of the mass, $a^{1/2}$ and $(ab/c)^{1/2}$ are the resonant frequencies in the low and high amplitude limits, respectively. The dissipation, assumed independent of drive, is represented by $k = (ab/c)^{1/2}/Q$ where Q is the quality factor. The oscillator is driven at frequency ω with amplitude G. Assuming a solution of the form $z = x\cos\omega t + y\sin\omega t$ leads to third order polynomial equations for x and y when higher harmonic terms (whose presence was searched for but could not be detected) are neglected. The coupled equations may be solved for x and y.

The observed frequency response of Figs. 1(a)–1(c) was fitted with the mechanical oscillator solution by adjusting parameters a, b/c, G, and k. Since ab/c and Q may be set by the large drive limit response, there are two remaining adjustable parameters. The fitted response (with $a^{1/2} = 2\pi \times 94.3\ \mathrm{s}^{-1}$, $b/c = 0.793$, $G = 3.1 \times 10^4$, and $Q = 90$), shown in Fig. 1, gives a fair representation of the observed 1.15 V drive data. It can be seen that the observed sweep-direction dependence of the response comes from the double-valued response of such a nonlinear oscillator. The slightly rounded response observed at both f_{up} and f_{down} (where a discontinuity is expected from the model) becomes sharper at higher temperatures and is not well understood. The fitting parameters for the 2.6 V drive data are kept the same as for 1.15 V except for the drive level parameter G which was simply increased proportionately to the drive.

By keeping all parameters (except G) fixed to the values that gave a good fit to 1.15 V drive data in Fig. 1, the values of f_{up}, f_{down}, M_{up}, and M_{down} were obtained as functions of drive from the response curves generated from the mechanical model solutions. The lines in Fig. 2 represent smoothed curves through these values. The model solution describes the observed rapid increase (decrease) in f_{up} (M_{up}) in the interesting small flow range. It also describes the observed smaller change in f_{down} and nearly linear change in M_{down} in the small flow range. As the drive level in the model is increased beyond 1.5 V, f_{up} becomes greater than f_{down}. Similarly M_{up} exhibits a kink as the hysteretic response begins to disappear. In the high drive limit, the solution to our mechanical model gives a single-valued response in contrast to the observed sweep-direction dependent response. Though small, the origin of the sweep-direction dependence in the high drive limit is not understood within this model. In spite of its simplicity, the mechanical model gives a fairly good description of our observations.

The question of how the $\hat{\mathbf{l}}$ texture changes as v_s is increased will now be addressed. To review briefly [4], recall that the order parameter of the A_1 phase may be defined using two triads of real orthogonal unit vectors, $(\hat{\mathbf{d}}, \hat{\mathbf{e}}, \hat{\mathbf{f}} = \hat{\mathbf{d}} \times \hat{\mathbf{e}}$ in spin space, and $(\hat{\mathbf{m}}, \hat{\mathbf{n}}, \hat{\mathbf{l}} = \hat{\mathbf{m}} \times \hat{\mathbf{n}})$ in orbital space. Minimizing the magnetic free energy while taking into account the anisotropy of the magnetic susceptibility shows that $\hat{\mathbf{f}}$ is directed along the applied magnetic field $\mathbf{H}$ ($\parallel \hat{\mathbf{z}}$) and, therefore, the unit vectors $(\hat{\mathbf{d}}, \hat{\mathbf{e}})$ are forced into the $\hat{\mathbf{x}}$-$\hat{\mathbf{y}}$ plane. The orientation dependent part of the dipolar interaction energy between Cooper pairs can be written as $(g(\hat{\mathbf{f}} \cdot \hat{\mathbf{l}})^2$, where g is a positive constant. The dipolar energy is then minimized when $\hat{\mathbf{f}} \perp \hat{\mathbf{l}}$ and the $\hat{\mathbf{l}}$ vector is also forced into the $\hat{\mathbf{x}}$-$\hat{\mathbf{y}}$ plane. The relative orientation of $\hat{\mathbf{l}}$ with respect to $(\hat{\mathbf{d}}, \hat{\mathbf{e}})$ in the $\hat{\mathbf{x}}$-$\hat{\mathbf{y}}$ plane is arbitrary in the A_1 phase (unlike in A and A_2).

To determine the equilibrium $\hat{\mathbf{l}}$ vector texture in the $\hat{\mathbf{x}}$-$\hat{\mathbf{y}}$ plane, the sum of kinetic and bending energy contributions to the total free energy is minimized subject to the constraint that $\hat{\mathbf{l}}$ be perpendicular to the boundaries [1,11]. The kinetic energy density is written as $F_{\mathrm{kin}} = (1/2)\rho(\rho_s/\rho_n)_{\alpha\beta} v_{s\alpha} v_{s\beta}$ (summation over repeated indices is implied). The bending free energy can be expressed as a sum of combinations of products of gradients in ψ, ϕ, and θ, defined as $\psi = \cos^{-1}(\hat{\mathbf{x}} \cdot \hat{\mathbf{d}})$, $\phi = \cos^{-1}(\hat{\mathbf{z}} \cdot \hat{\mathbf{n}})$, and $\theta = \cos^{-1}(\hat{\mathbf{x}} \cdot \hat{\mathbf{l}})$. In the presence of superfluid component flow in the A_1 phase, the broken relative spin-orbital gauge symmetry requires that $v_{s\alpha} = (\hbar/2m)(\hat{\mathbf{m}} \cdot \partial\hat{\mathbf{n}}/\partial\alpha + \hat{\mathbf{d}} \cdot \partial\hat{\mathbf{e}}/\partial\alpha) = -(\hbar/2m)(\partial\psi/\partial\alpha - \partial\phi/\partial\alpha)$ [3]. Taking $\hat{\mathbf{q}}$ and $\mathbf{v}_s$ to be along the $\hat{\mathbf{x}}$ direction,

we obtain $F_{\rm bend}/F_0 = (4m^2v_s^2/\hbar^2)(3 - \cos2\theta) + \theta_x'^2(2 + \cos2\theta) + \theta_y'^2(2 - \cos2\theta) + 2\theta_x'\theta_y'\sin2\theta + \theta_z'^2 + (4mv_s\theta_z'/\hbar)\cos\theta$, where $\theta_\alpha' \equiv \partial\theta/\partial\alpha$, $F_0 = 3\hbar^2N\rho_{s\parallel}(1 + F_1/3)/32m^*\rho$, N the number density, F_1 a Fermi liquid parameter, and m^* effective mass of ^{3}He. The equilibrium texture in the $F_{\rm kin} = 0$ limit was previously solved by numerical methods on a two dimensional square grid [12]. We incorporate the kinetic contribution through an adjustable healing length parameter ξ and require that our solution reproduces that of Ref. [12], in the limit of zero flow and for square boundary [13]. For given v_s the total free energy was evaluated as a function of ξ by integrating over the volume of the cylinder. The total free energy was minimized at a unique value of ξ which specified the equilibrium texture for the given v_s [13]. The calculated equilibrium texture for $v_s = 8$ μm/s is shown in the inset of Fig. 3.

A full analysis of the transducer response in terms of the calculated texture is quite complicated in detail. It is found, however, that the essential physics may be captured using a simple v_s dependent volume-averaged superfluid density $\bar{\rho}_s$ which is evaluated for the texture using Eq. (2). The ratio $\bar{\rho}_s/\rho_{s\perp}$ (where $\rho_{s\perp} = 2\rho_{s\parallel}$) is shown as a function of v_s in Fig. 3. The low flow linear response region is limited to small $v_s \lesssim 2$ μm/s. At high velocities, the texture tends to saturate as the cost in $F_{\rm bend}$ grows. If $\hat{\mathbf{l}}$ becomes parallel to $\hat{\mathbf{q}}$ throughout the cell, $\bar{\rho}_s/\rho_{s\perp}$ would be 1/2. Figure 3 demonstrates that the average superfluid density seen by the spin-entropy wave decreases and eventually saturates as v_s is increased. This is consistent with our observations. The amplitude dependence of the superfluid density is analogous to the "spring constant," $a(1 + bz^2)/(1 + cz^2)$, in our mechanical model. The amplitude dependence of the spring constant resembles that of $\bar{\rho}_s/\rho_{s\perp}$.

According to the estimate of our transducer calibration, the superfluid component velocity amplitude would be 43 μm/s at $D = 2.6$ V in Fig. 2. At this velocity the calculated $\bar{\rho}_s/\rho_{s\perp}$ is 0.52 as seen in Fig. 3. The estimated $\bar{\rho}_s$ from the measured f_{up} at the same D and the $\rho_{s\perp}$ measured earlier [5] under the same conditions of magnetic field, pressure, and temperature give $\bar{\rho}_s/\rho_{s\perp} = 0.54$. This is close to the calculated value of the ratio.

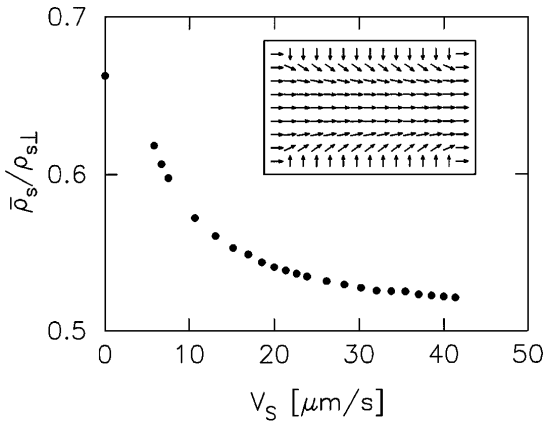

FIG. 3. Calculated $\bar{\rho}_s/\rho_{s\perp}$ for the equilibrium texture as a function of superflow velocity. Inset: $\hat{\mathbf{l}}$ texture when $v_s = 8$ μm/s.

In conclusion, we have observed nonlinear propagation of spin-entropy (second sound) waves in ^{3}He-A_1 filling a resonator. The salient features of this phenomenon are consistent with the sound generated superflow altering the $\hat{\mathbf{l}}$ texture within the resonator, thereby modifying the volume-averaged propagation velocity.

We thank Yuichi Okuda for helping us in setting up our spin-entropy wave apparatus. The help from H. Zapolsky was crucial to constructing the mechanical model presented. This research is supported by NSF Grant No. DMR9510306.

*Permanent address: Mikroelektronik Centret, Danish Technical University, DK 2800 Lyngby, Denmark.

[1] D. Vollhardt and P. Wölfle, *The Superfluid Phases of Helium* (Taylor and Francis, London, 1990), Vol. 3.
[2] P. G. N. de Vegvar *et al.*, Phys. Rev. Lett. **57**, 1028 (1986).
[3] M. Liu, Phys. Rev. Lett. **43**, 1740 (1979).
[4] A. J. Leggett, Rev. Mod. Phys. **47**, 331 (1975).
[5] M. Bastea, Y. Okuda, V. LaBella, and H. Kojima, Phys. Rev. Lett. **73**, 1126 (1994).
[6] M. Liu, Phys. Rev. B **29**, 2833 (1984).
[7] U. E. Israelsson, B. C. Crooker, H. M. Bozler, and C. M. Gould, Phys. Rev. Lett. **53**, 1943 (1984); **54**, 254(E) (1985).
[8] The second resonant mode was also studied. In addition to the main nonlinear and hysteretic behavior similar to the first mode, other hysteretic abrupt but smaller changes in response were observed on the higher side of the resonant peak. These smaller features did not occur reproducibly. A more complicated superflow field in the second mode probably induces metastable states. Though searched for, no resonancelike response was found at third and greater harmonics.
[9] See, for example, L. D. Landau and E. M. Lifshitz, *Mechanics* (Pergamon Press, London, 1959).
[10] This form of equation of motion was suggested to us by Harry Zapolsky. It allows us to conveniently solve for the response using MATHEMATICA.
[11] In the analysis, the orbital relaxation time is assumed much longer than the period of spin-entropy wave generated superflow and that the texture is stationary during the flow cycle. Estimates of the orbital relaxation time for our experimental conditions indicate the assumption is well satisfied.
[12] P. G. N. de Vegvar, Ph.D. thesis, Cornell University, 1986 (unpublished).
[13] M. Bastea and H. Kojima, J. Low Temp. Phys. **101**, 733 (1995). The Euler-Lagrange equation for minimizing the total free energy was checked for our equilibrium textures with finite v_s and was found to be satisfied to the same accuracy as with $v_s = 0$.